Available online at www.sciencedirect.com
ScienceDirect
Journal of the European Ceramic Society 28 (2008) 1679–1685
www.elsevier.com/locate/jeurceramsoc

Microstructure and properties of bulk Ta_2AlC ceramic synthesized by an *in situ* reaction/hot pressing method

Chunfeng Hu [a,b], Lingfeng He [a,b], Jie Zhang [a,b], Yiwang Bao [a], Jingyang Wang [a], Meishuan Li [a], Yanchun Zhou [a,*]

[a] *Shenyang National Laboratory for Materials Science, Institute of Metal Research, Chinese Academy of Sciences, 72 Wenhua Road, Shenyang 110016, China*
[b] *Graduate School of Chinese Academy of Sciences, Beijing 100039, China*

Received 6 June 2007; received in revised form 15 October 2007; accepted 26 October 2007
Available online 4 March 2008

Abstract

Dense bulk Ta_2AlC ceramic was synthesized by an *in situ* reaction/hot pressing method using Ta, Al, and C as initial materials. The average grain size of Ta_2AlC is 15 μm in length and 3 μm in width. The physical and mechanical properties were investigated. Ta_2AlC is a good electrical and thermal conductor. The flexural strength and fracture toughness of Ta_2AlC were measured to be 360 MPa and 7.7 MPa m$^{1/2}$, respectively. The typical layered grains contribute to the damage tolerance of this ceramic. After indentation up to 200 N at the tensile surface of the beam specimens, no obvious decrease of the residual flexural strength was observed. Even at above 1200 °C, Ta_2AlC still retains a high Young's modulus and shows excellent thermal shock resistance, which renders it a promising high-temperature structural material.

Keywords: Ta_2AlC; Hot pressing; Electrical conductivity; Thermal conductivity; Mechanical properties

1. Introduction

$M_{n+1}AX_n$ (where M is an early transition metal, A is an A group element, X is C or N, and n = 1–3), also called MAX phases, is a family of ternary phases with hexagonal structure.[1,2] They are electrically and thermally conductive, machinable, damage tolerant, and resistant to thermal shock, and promising for high-temperature applications.[3–7] When n is 1, A is Al, and X is C, M_2AlC phases are represented. Recently, the synthesis and characteristics of Ti_2AlC,[8–10] Cr_2AlC,[11,12] V_2AlC,[13] Nb_2AlC,[14,15] Ta_2AlC,[16–20] etc. have been investigated. For Ta_2AlC, Sun et al.[16] calculated the elastic modulus of 318.6 GPa and density of 11.52 g cm^{-3} by *ab initio* total energy calculations. Manoun et al.[17] found that the compressibilities of Ta_2AlC along the c axis and along a axis were almost identical. Lin et al.[18] confirmed the layered microstructure feature of Ta_2AlC by high resolution transmission electron microscopy. Gupta et al.[19] identified that Ta_2AlC had poor oxidation resistance. Very recently, Gupta et al.[20] found that Ta_2AlC/Ag-based composite showed the good tribological performance over a wide temperature range against Ni-based superalloys and alumina. However, to the author's knowledge, there are seldom reports on the physical and mechanical properties of Ta_2AlC. As a potential high-temperature structural ceramic, it is necessary to understand the intrinsic physical and mechanical characteristics of Ta_2AlC. In this paper, dense bulk Ta_2AlC was fabricated by an *in situ* reaction/hot pressing method using Ta, Al, and C powders as initial powders. The electrical resistivity was investigated in a temperature range of 10–300 K. The molar heat capacity and thermal conductivity, as well as mechanical properties, were determined from ambient temperature to 1500 K. The physical and mechanical properties were compared with those of other Al-containing 211 phases, such as Ti_2AlC and Cr_2AlC.

2. Experimental details

Commercial powders of tantalum (−200 mesh, 99%), aluminum (−300 mesh, 99%), and graphite (−200 mesh, 99%) were used as initial materials for fabricating Ta_2AlC. The as-

* Corresponding author. Tel.: +86 24 23971765; fax: +86 24 23891320.
E-mail address: yczhou@imr.ac.cn (Y. Zhou).

0955-2219/$ – see front matter © 2007 Elsevier Ltd. All rights reserved.
doi:10.1016/j.jeurceramsoc.2007.10.006

received Ta, Al, C powders with molar ratio of 2:1.2:0.9 were weighed and ball-milled in an agate jar for 12 h. After sieving with a 100-mesh screen, the mixture of powders was uniaxially pressed in a BN-coated graphite die under 5 MPa. Then the green compact was heated to 1550 °C with a heating rate of 15 °C min^{-1} in a flowing Ar atmosphere. The sample was held at 1550 °C for 30 min under a pressure of 30 MPa, and then annealed at 1400 °C for 60 min. At last, the sample was cooled down to room temperature with the furnace cooling rate. The contaminations on the surface were removed using a high-speed running grinding wheel.

The density of as-prepared Ta_2AlC sample, measured by the Archimedes principle, yields 11.46 g cm^{-3}, which is close to the theoretical value of 11.52 g cm^{-3}. Phase compositions were determined by X-ray diffraction (XRD) (Rigaku D/max-2400, Tokyo, Japan) utilizing Cu Kα radiation (λ = 1.54178 Å) at a scanning speed of 0.04°/step. The measurement of grain size was conducted using a grain-intercept method. The polished surface of Ta_2AlC sample was etched in an acid solution consisting of HF, HNO_3, and H_2O mixed at an equal volume fraction, and then was observed by a scanning electron microscope (SEM) (LEO Supra35, Oberkochen, Germany) equipped with an energy dispersive spectroscopic (EDS) system. At least fifty grains were measured. The microstructure of Ta_2AlC was investigated by SEM. Thin-foil sample for transmission electron microscope (TEM) investigation was prepared by slicing, grinding to ∼20 μm, dimpling down to ∼10 μm and ion milling at 4 kV. The microstructure features were observed by a 300 kV Tecnai G^2 F30 TEM (FEI Co., Eindhoven, Netherland).

All specimens used for the physical and mechanical tests were machined by an electrical discharged method (EDM), and then ground and polished down to 1.0 μm diamond grits. The electrical conductivity of Ta_2AlC was measured in a temperature range of 10–300 K by a four-point probe method in a superconducting quantum interference device (SQUID) (Quantum Design, San Diego, USA), using a sample with a dimension of 1 mm × 1 mm × 10 mm. The thermocouple sticking to the sample could instantaneously measure the temperature of sample. The test current was 10 mA. The thermal expansion coefficient (TEC) of Ta_2AlC was measured by a thermal mechanical analyzer (TMA) (Setsys 24, Caluire, France) under a flowing Ar atmosphere from ambient temperature to 1100 °C with a heating rate of 2 °C min^{-1}, using a column specimen of 6 mm in diameter and 8 mm in length. The temperature conductivity coefficient and molar heat capacity of Ta_2AlC were measured using a disk sample with a dimension of Φ12.7 mm × 1.5 mm by a Flashline^{TM}-5000 thermal properties analyzer (Anter Corp., Pittsburgh, USA). The thermal conductivity, λ (W m^{-1} K^{-1}), was calculated based on the equation[12]:

$$\lambda = \alpha \frac{c_p d}{M} \times 10^{-1} \quad (1)$$

in which α is the coefficient of temperature conductivity (cm^2 s^{-1}), c_p the molar heat capacity (J mol^{-1} K^{-1}), d the density (g cm^{-3}) and M the molar mass (kg mol^{-1}).

The flexural strength was measured using a three-point bending method and the fracture toughness was measured using single-edge notched beams (SENB). The specimen size for flexural strength is 3 mm × 4 mm × 36 mm and that for fracture toughness measurement is 4 mm × 8 mm × 36 mm. The notch machined by EDM is 4 mm in length and ∼0.15 mm in width with the notch radius of ∼0.03 mm. The crosshead speeds for flexural strength and fracture toughness tests were

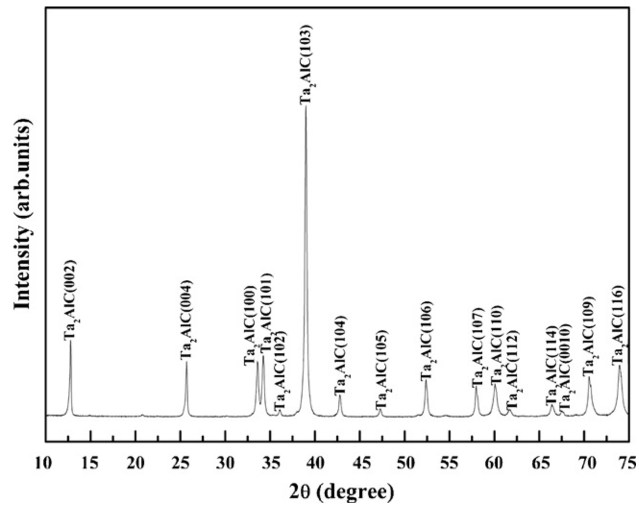

Fig. 1. X-ray diffraction pattern of Ta_2AlC synthesized by an *in situ* reaction/hot pressing method.

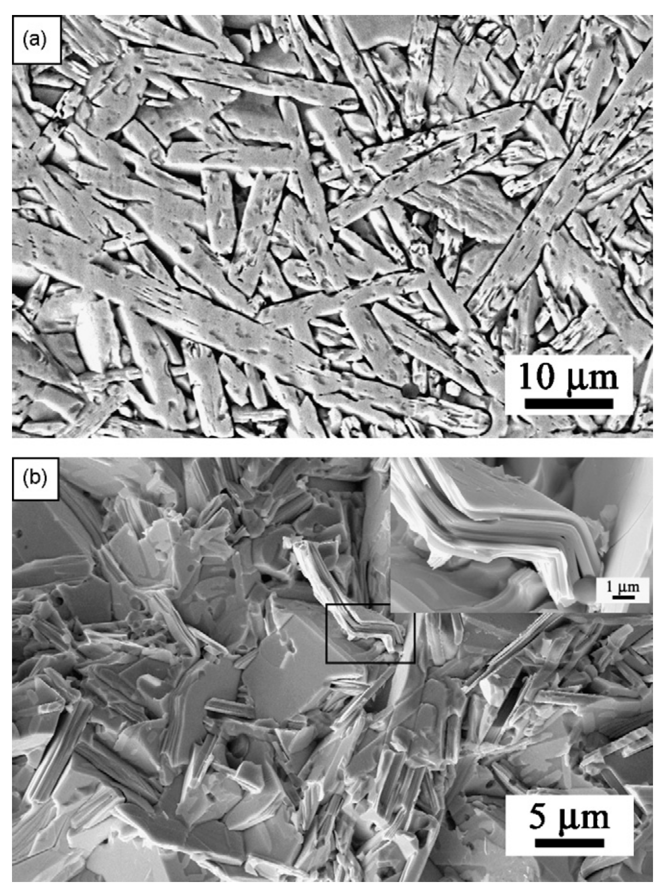

Fig. 2. Scanning electron microscope (SEM) micrographs of (a) etched surface and (b) fractured surface of Ta_2AlC. The magnification in (b) shows typical kink bands.

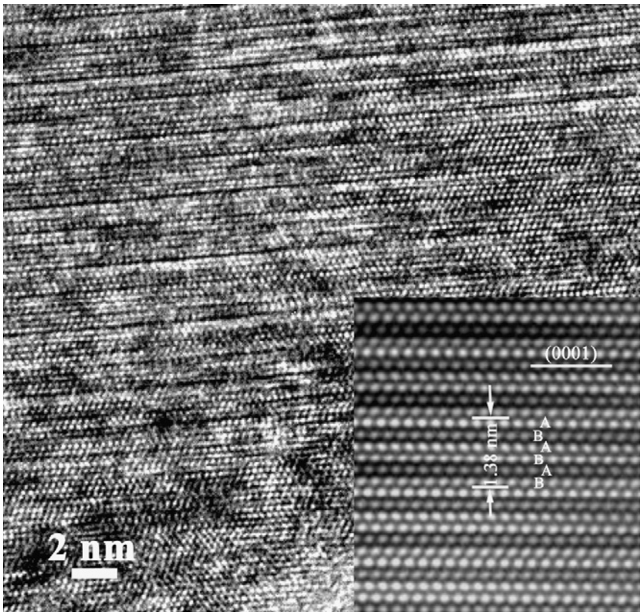

Fig. 3. HRTEM micrograph of Ta_2AlC. The viewing direction is $[1\,\bar{2}\,1\,0]$. The inset shows the arrangements of two Ta layers per Al layer.

0.5 and 0.05 mm min^{-1}, respectively. To understand the toughening mechanisms, *in situ* cracks were produced according to the pre-cracking method developed by Bao and Zhou.[21] Vickers hardness was measured by a microhardness tester at loads of 0.5, 2, 10, 30, and 50 N with a dwell time of 15 s. The indents were investigated by SEM. The damage tolerance was evaluated by testing the post-indentation residual flexural strength after indenting at loads of 100, 200, and 300 N at the middle span of the 3 mm × 4 mm × 36 mm samples. The indent sizes were measured through an optical microscope. Measurement of shear strength was conducted by a punch-shear method.[22] The average thickness of thin plate is 0.1 mm and the ratio of thickness to diameter of the punch hole is ~0.1. The crosshead speed is 0.5 mm min^{-1}. The shear-fractured surface was observed by SEM.

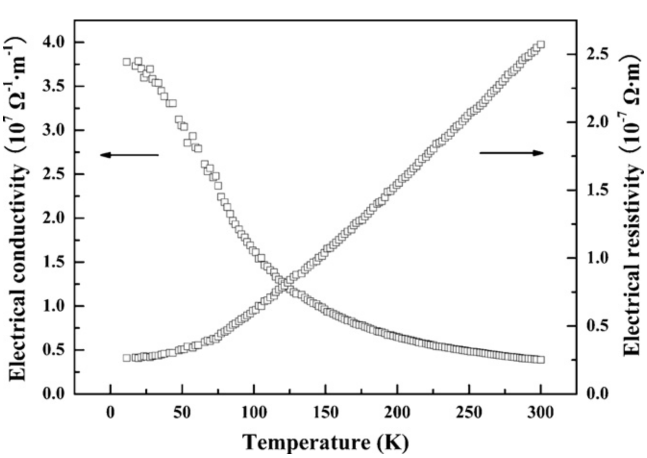

Fig. 4. Evolutions of electrical conductivity and electrical resistivity of Ta_2AlC in the temperature range of 10–300 K.

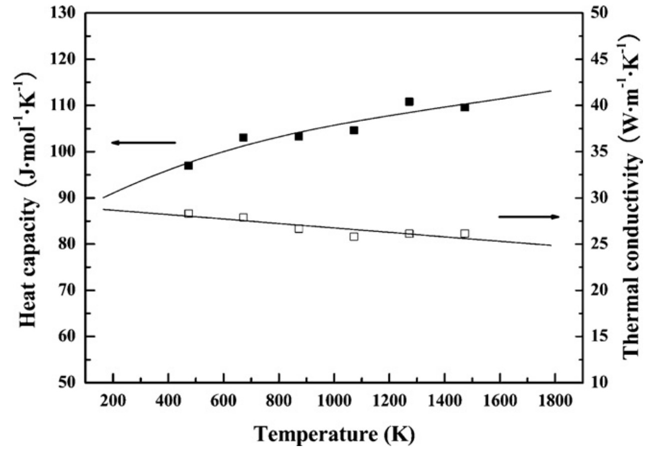

Fig. 5. Temperature dependence of molar heat capacity and thermal conductivity of Ta_2AlC.

Temperature dependence of Young's modulus of Ta_2AlC was performed by an impulse excitation technique (IET). A specimen with a dimension of 3 mm × 15 mm × 40 mm was heated in a HTVP-1750-C furnace (IMCE, Diepenbeek, Belgium) with a heating rate of 3 °C min^{-1} up to 1200 °C in vacuum on the order of 10^{-3} mbar. Thermal shock resistance of Ta_2AlC was tested in air by annealing the samples (3 mm × 4 mm × 36 mm) at the testing temperature for 15 min, and then immediately quenching in the ambient water. The testing temperatures were 400, 600, 800, 1000, and 1200 °C, respectively. The retained flexural strength was measured by a three-point bending method in a universal testing machine. The cross-sectioned surface of quenched samples was investigated by SEM.

3. Results and discussion

3.1. Microstructure

By XRD analysis, Ta_2AlC is determined as the predominant phase in as-prepared sample, as shown in Fig. 1. Fig. 2 shows the etched surface and fracture surface of Ta_2AlC. The average size of plate-like grains of Ta_2AlC is 15 μm in length and 3 μm in width (Fig. 2(a)). Delamination, kinking, intergranular and transgranular fractures are revealed in Fig. 2(b). The insert is a magnification of the rectangular region, which shows the typical kink band in an individual grain. The microstructure feature was investigated by TEM. The atom arrangement of Ta_2AlC projected on a $(1\,\bar{2}\,1\,0)$ plane indicates the layer stacking sequence of Ta and Al atoms along the [0 0 0 1] direction, as shown in Fig. 3. The inset shows the atomic arrangements of two Ta layers and one Al layer alternately stack along the [0 0 0 1] direction. The Ta layers are separated by close packed Al atoms on (0 0 0 1) plane, and the stacking sequence of Ta and Al atoms is ABABAB. The weak Ta-Al bond[16] in Ta_2AlC suggests that shear deformation is along Al plane. So, the kink bands can be easily formed, which contributes to the plastic irreversible deformation of Ta_2AlC.[10,23–25]

Table 1
Typical physical and mechanical properties of Ta_2AlC, Ti_2AlC, and Cr_2AlC

Properties	Ta_2AlC	Ti_2AlC[2,8,9]	Cr_2AlC[11,12]
Lattice parameters (Å)	$a = 3.079$; $c = 13.854$	$a = 3.051$; $c = 13.637$	$a = 2.858$; $c = 12.818$
Density ($g\,cm^{-3}$)	11.46	4.11	5.21
Temperature coefficient of resistivity, β (K^{-1})	0.0042	0.0035	0.0028
Electrical conductivity ($\times 10^6\ \Omega^{-1}\,m^{-1}$)	3.91	4.42	1.4
Thermal expansion coefficient ($\times 10^{-6}\,K^{-1}$)	8.0	8.2	13.3
Heat capacity at 25 °C ($J\,mol^{-1}\,K^{-1}$)	93.6	78	84.3
Thermal conductivity at 25 °C ($W\,m^{-1}\,K^{-1}$)	28.4	46	17.9
Vickers hardness (GPa)	4.4 ± 0.1	2.8	3.5
Compressive strength (MPa)	804	763	–
Shear strength (MPa)	112 ± 24	–	–
Flexural strength (MPa)	360 ± 19	275	378
Fracture toughness ($MPa\,m^{1/2}$)	7.7 ± 0.2	6.5	–
Young's modulus (GPa)	292	305	278
Shear modulus (GPa)	121	127	116

3.2. Electrical and thermal properties

3.2.1. Electrical properties

Fig. 4 displays the temperature-dependent electrical conductivity and electrical resistivity of Ta_2AlC from 10 to 300 K. The relationship between electrical conductivity and electrical resistivity is

$$\rho = \frac{1}{\sigma} \tag{2}$$

in which ρ is the electrical resistivity ($\mu\Omega\,m$), σ the electrical conductivity ($\mu\Omega^{-1}\,m^{-1}$). At room temperature, the electrical conductivity of Ta_2AlC is $3.91 \times 10^6\ \Omega^{-1}\,m^{-1}$, which is 2.8 times higher than that of Cr_2AlC ($1.4 \times 10^6\ \Omega^{-1}\,m^{-1}$)[12] and close to that of Ti_2AlC ($4.6 \times 10^6\ \Omega^{-1}\,m^{-1}$).[2] The total density of state (DOS) at Fermi level of Ta_2AlC (2.98 $(eV\,cell)^{-1}$) is lower than those of Cr_2AlC (6.83 $(eV\,cell)^{-1}$) and Ti_2AlC (3.10 $(eV\,cell)^{-1}$), which indicates the lack of carriers in Ta_2AlC.[26] However, the higher electrical conductivity of Ta_2AlC, compared with Cr_2AlC, may result from the higher mobility of carriers.[26] With the increasing temperature, the electrical conductivity of Ta_2AlC decreases from 37.8×10^6 to $3.89 \times 10^6\ \Omega^{-1}\,m^{-1}$. It is seen that the electrical resistivity increases linearly above 75 K, indicating a metallic characteristic of Ta_2AlC.[2,5] Fitting the resistivity with temperature ranging from 75 to 300 K, we obtain an expression:

$$\rho(\mu\Omega\,m) = \rho_0(1 - \beta\Delta T) = 0.229[1 - 0.0042(273.15 - T)] \tag{3}$$

in which ρ_0 is the electrical resistivity at 273.15 K ($\mu\Omega\,m$), β the temperature coefficient of resistivity (K^{-1}) and T the absolute temperature (K). The temperature coefficient of resistivity is $0.0042\,K^{-1}$, which is higher than those of Ti_2AlC ($0.0035\,K^{-1}$)[2] and Cr_2AlC ($0.0028\,K^{-1}$).[12]

3.2.2. Thermal properties

The average thermal expansion coefficient (TEC) of Ta_2AlC tested from room temperature to 1100 °C is $8.0 \times 10^{-6}\,K^{-1}$, which is lower than those of Ti_2AlC ($8.2 \times 10^{-6}\,K^{-1}$)[8] and Cr_2AlC ($13.3 \times 10^{-6}\,K^{-1}$).[12] Fig. 5 presents temperature dependence of molar heat capacity and thermal conductivity of Ta_2AlC. It is seen that the molar heat capacity of Ta_2AlC increases with temperature following a third-order polynomial and approaches to a constant. At ambient temperature, the molar heat capacity of Ta_2AlC is $93.6\,J\,mol^{-1}\,K^{-1}$, which is higher than those of Ti_2AlC ($78\,J\,mol^{-1}\,K^{-1}$)[8] and Cr_2AlC ($84.3\,J\,mol^{-1}\,K^{-1}$).[12] A linear fitting of the thermal conductivity of Ta_2AlC with temperature yields a function:

$$\lambda = 29.16031 - 0.00241T \tag{4}$$

with a coefficient of determination, r^2, of 0.98. The thermal conductivity decreases linearly with increasing temperature. From ambient temperature to 1227 °C, the thermal conductivity decreases from 28.4 to $25.5\,W\,m^{-1}\,K^{-1}$, which is similar to those of Ti_2AlC[8] and Cr_2AlC.[12] At room temperature, the thermal conductivity of Ta_2AlC is $28.4\,W\,m^{-1}\,K^{-1}$, which is higher than that of Cr_2AlC ($17.9\,W\,m^{-1}\,K^{-1}$),[12] but lower than that of Ti_2AlC ($46\,W\,m^{-1}\,K^{-1}$).[2] Additionally, it is known that the total thermal conductivity is associated with both the electronic and phonon contributions ($\lambda_{total} = \lambda_{electron} + \lambda_{phonon}$).[2] At 25 °C, the calculated $\lambda_{electron}$ of Ta_2AlC based on the Wiedmann–Franz Law ($\lambda_{electron} = L_0\sigma T$, where σ is the electrical conductivity at the Kelvin temperature, T, and $L_0 = 2.45 \times 10^{-8}\,W\,\Omega\,K^{-2}$)[2] is $28.3\,W\,m^{-1}\,K^{-1}$, which is nearly equal to the experimental total thermal conductivity of $28.4\,W\,m^{-1}\,K^{-1}$. Therefore, it is concluded that the electrons mainly contribute to the conductivity of Ta_2AlC at room temperature.

3.3. Mechanical properties

3.3.1. Flexural strength and fracture toughness

Table 1 summarizes the measured physical and mechanical properties of Ta_2AlC together with those of Ti_2AlC and Cr_2AlC. The flexural strength of Ta_2AlC evaluated by a three-point bending method is 360 MPa, which is higher than that of Ti_2AlC (275 MPa)[9] but slightly lower than that of Cr_2AlC (378 MPa).[12] The fracture toughness of Ta_2AlC determined on the SENB samples ($7.7\,MPa\,m^{1/2}$) is higher than that of Ti_2AlC ($6.5\,MPa\,m^{1/2}$).[9] Therefore, Ta_2AlC shows improved flexural

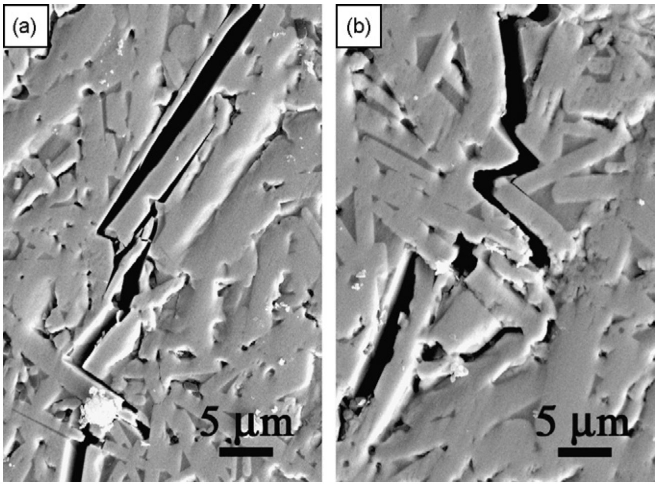

Fig. 6. Crack propagation on the polished surface of Ta_2AlC, showing the toughening mechanisms: (a) grains pull-out and bridging and (b) crack zigzag deflection.

strength and fracture toughness compared with Ti_2AlC at room temperature.

Wang and Zhou[5] reported the tortuous crack path as well as the bridging and pull-out of Ti_3AlC_2 grains resulted in a rough fracture surface and high fracture toughness. In order to investigate the toughening mechanisms of Ta_2AlC, *in situ* cracks were produced based on pre-cracking method,[21] as shown in Fig. 6. Similarly, the zigzag propagation of cracks together with bridging and pull-out of Ta_2AlC grains were observed, which results in a rough fracture surface and high toughness.

3.3.2. Vickers hardness, damage tolerance and shear strength

Fig. 7 shows the Vickers hardness as a function of testing load. The hardness is load-dependent. With increasing load from 0.5 to 50 N, the hardness gradually decreases from 9.1 to 4.4 GPa. Such a phenomenon is sometimes referred to as *Indentation-Size Effect* (ISE).[27–29] Similarly, this tendency has been observed

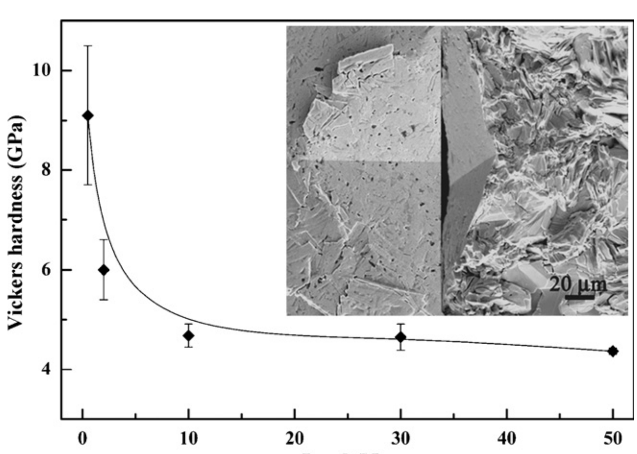

Fig. 7. Vickers hardness of Ta_2AlC versus indentation load at ambient temperature, and SEM micrograph of a hardness indent (50 N).

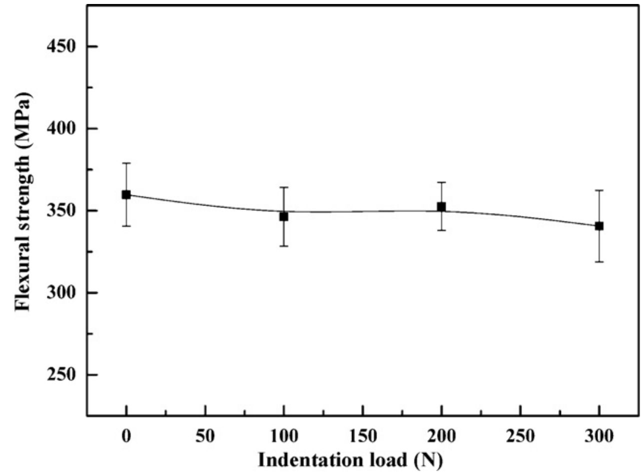

Fig. 8. Indentation load dependence of residual flexural strength of Ta_2AlC.

in Ti_2AlC[9] and Cr_2AlC.[11] At a lower load, the bigger scatter may be attributed to the anisotropic nature of grains.[3,5] It is seen that the hardness value inclines to a constant above 10 N load. Therefore, the intrinsic hardness of Ta_2AlC is close to 4.4 GPa, which is higher than that of Ti_2AlC (2.8 GPa)[9] and Cr_2AlC (3.5 GPa).[12] The Vickers indent produced at a load of 50 N (see the inset of Fig. 7) shows that no cracks emanate from the diagonals of indent. The cross-section of indent reveals that the damage is constrained in a local district with multiple energy-absorbing mechanisms of delamination, grains push-out, intergranular and transgranular fractures. Low[30] demonstrated that the micro-damage of Ti_3SiC_2 was widely distributed within the shear-compression zone around and below the Vickers contacts. Bao et al.[31] observed that the indentation on the layered ceramic resulted in lax grains at the indent perimeter, rather than brittle cracks at the corners of the indent. It is concluded that Ta_2AlC has similar quasi-plasticity with Ti_3SiC_2.

From previous reports,[2–4] it is known that Ti_3SiC_2 is damage tolerant. Below a critical load value, the post-indentation flexural strengths of Ti_3SiC_2 are almost independent of indentation loads.[2,3,7] We expect that Ta_2AlC should also have the damage tolerance. The experimental results of indentation load dependent residual flexural strength of Ta_2AlC are displayed in Fig. 8. It is seen that below 200 N (indent size, 335 μm), the residual flexural strength of Ta_2AlC samples does not degrade with increasing indentation load. Even under the Vickers contact damage of 300 N (indent size, 397 μm), the residual flexural strength still maintains about 94% of that of undamaged samples. The indent size is about 10% of the sample's width. It is proven that Ta_2AlC is damage tolerant and insensitive to the defects produced at indentation load less than 200 N. In other words, Ta_2AlC is insensitive to a defect smaller than 335 μm.

In addition, the measured shear strength of Ta_2AlC is low, only 112 MPa. It is observed that the punch-shear holes show perfect shapes without macrocracks emanating and propagating, which indicates the machinable capability. In the fracture surface (not shown for brevity), the fragmented debris as well as transgranular fractured grains is observed.

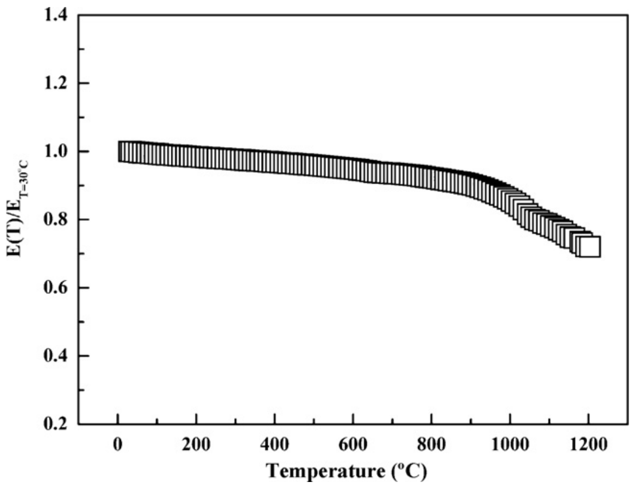

Fig. 9. Temperature dependence of normalized Young's modulus of Ta_2AlC.

3.3.3. High-temperature Young's modulus and thermal shock resistance

Young's modulus of Ta_2AlC as a function of temperature is plotted in Fig. 9. Below 900 °C, a slowly linear decrease is observed with increasing temperature. Whereas, there is a break at temperature between 900 and 1000 °C. Above 1000 °C, more rapid decrease of Young's modulus is observed with increasing temperature. However, even up to 1200 °C, the modulus loss of Ta_2AlC is only 28%, which demonstrates the high-temperature stiffness of this ceramic.[32] The thermal shock resistance was also investigated by measuring the retained strength after quenching. Fig. 10 shows the residual flexural strength of Ta_2AlC as a function of quenching temperature. When quenching at 600 °C, the retained flexural strength has a lowest value of 230 MPa, which is about 64% of unquenched ones. Bao et al.[33] determined that the strength degradation was probably ascribed to water infiltration that led to the grain boundary weakness. Similarly, the loose grains in surface layer of Ta_2AlC when quenching at 600 °C are observed, as shown in Fig. 11(a). When increasing the quenching temperature, the abnormal thermal shock behavior of Ta_2AlC appears. Up to 1200 °C, the residual flexural strength of Ta_2AlC increases to 308 MPa. Zhang et al.[6] proved that surface oxide layers essentially acted as thermal barriers that reduced the surface heat transfer coefficient so that the transient tensile stresses in the substrate was decreased. In Fig. 11(b), it is seen that when quenching at 1000 °C, some microcracks only distribute in the outer oxidation layer (Ta_2O_5 and $AlTaO_4$) of Ta_2AlC, and the substrate keeps integrity. Therefore, the high residual flexural strength of Ta_2AlC can be obtained, showing excellent thermal shock resistance.

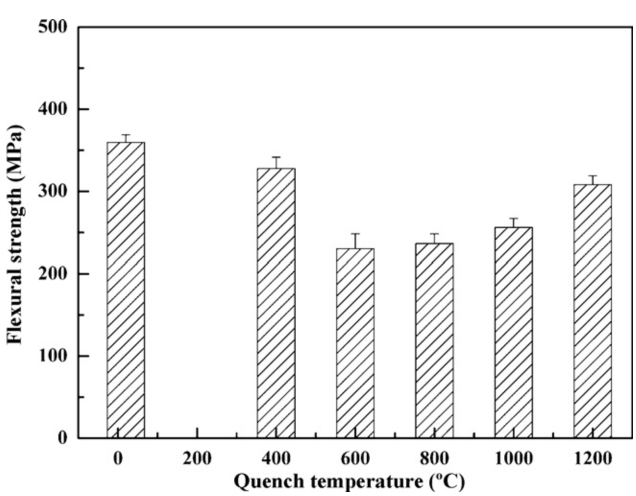

Fig. 10. Residual flexural strength of Ta_2AlC as a function of quenching temperature.

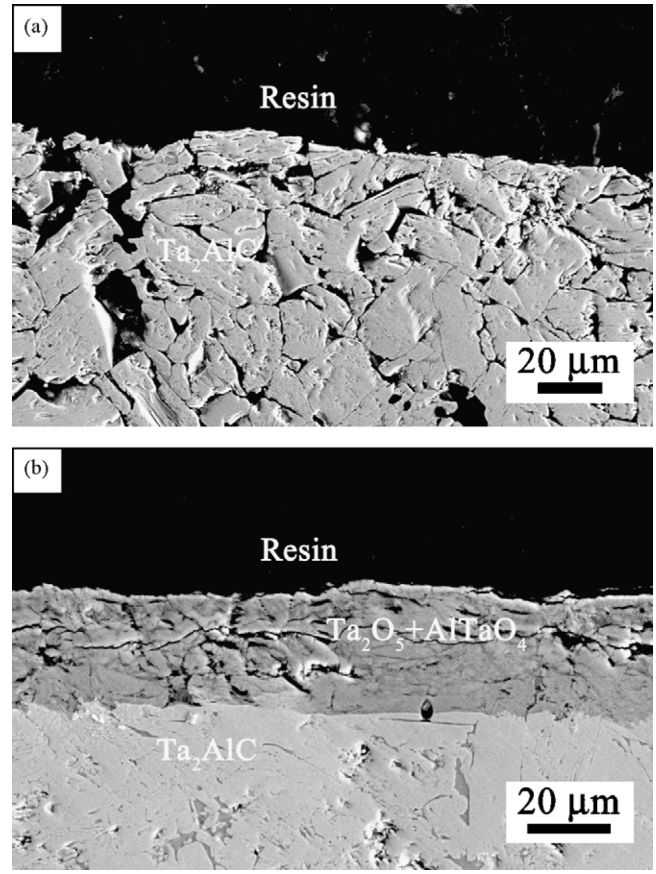

Fig. 11. SEM micrographs of cross-sectioned surface of Ta_2AlC samples quenching at (a) 600 °C and (b) 1000 °C.

4. Conclusions

Laminar-grained Ta_2AlC ceramic was fabricated by an *in situ* reaction/hot pressing method using Ta, Al, and C as initial materials. Ta_2AlC is demonstrated to be a good electrical and thermal conductor. In the temperature range of 10–300 K, the electrical conductivity decreases from 37.8×10^6 to $3.89 \times 10^6\ \Omega^{-1}\ m^{-1}$; and from ambient temperature to 1227 °C, thermal conductivity decreases from 28.4 to 25.5 $W\ m^{-1}\ K^{-1}$. Ta_2AlC also exhibits the typical mechanical properties like other layered ternary carbides. Ta_2AlC possesses low Vickers hardness of 4.4 GPa, shear strength of 112 MPa, high compressive strength of 804 MPa, and fracture toughness of 7.7 $MPa\ m^{1/2}$. Below 200 N indentation load in the middle span of a beam specimen, no decrease of residual flexural strength of Ta_2AlC samples is observed, indicating the good damage tolerance. Up to 1200 °C, Ta_2AlC still remains high Young's modulus and shows excellent thermal shock resistance.

Acknowledgements

This work was supported by the National Outstanding Young Scientist Foundation (No. 59925208 for Y.C. Zhou and No. 50125204 for Y.W. Bao), Nature Science Foundation of China under Grant No. 50232040, No. 50302011, No. 90403027, Chinese Academy of Sciences and French Atomic Energy Commission.

References

1. Nowotny, H., Struktuchemie einiger verbindungen der ubergangsmetalle mit den elementen C, Si, Ge, Sn. *Prog. Solid State Chem.*, 1970, **2**, 27.
2. Barsoum, M. W., The $M_{N+1}AX_N$ phases: a new class of solids; thermodynamically stable nanolaminates. *Prog. Solid State Chem.*, 2000, **28**, 201–281.
3. Barsoum, M. W. and El-Raghy, T., Synthesis and characterization of a remarkable ceramic: Ti_3SiC_2. *J. Am. Ceram. Soc.*, 1996, **79**(7), 1953–1956.
4. Zhou, Y. C. and Sun, Z. M., Micro-scale plastic deformation of polycrystalline Ti_3SiC_2 under room-temperature compression. *J. Eur. Ceram. Soc.*, 2001, **21**, 1007–1011.
5. Wang, X. H. and Zhou, Y. C., Microstructure and properties of Ti_3AlC_2 prepared by the solid–liquid reaction synthesis and simultaneous *in situ* hot pressing process. *Acta Mater.*, 2002, **50**, 3141–3149.
6. Zhang, H. B., Zhou, Y. C., Bao, Y. W. and Li, M. S., Abnormal thermal shock behavior of Ti_3SiC_2 and Ti_3AlC_2. *J. Mater. Res.*, 2006, **21**(9), 2401–2407.
7. Wan, D. T., Zhou, Y. C., Hu, C. F. and Bao, Y. W., Improved strength-impairing contact damage resistance of $Ti_3Si(Al)C_2$/SiC composites. *J. Eur. Ceram. Soc.*, 2007, **27**, 2069–2076.
8. Barsoum, M. W., Ali, M. and El-Raghy, T., Processing and characterization of Ti_2AlC, Ti_2AlN and $Ti_2AlC_{0.5}N_{0.5}$. *Met. Mater. Trans.*, 2000, **31A**, 1857–1865.
9. Wang, X. H. and Zhou, Y. C., Solid–liquid reaction synthesis and simultaneous densification of polycrystalline Ti_2AlC. *Z. Metalkd.*, 2002, **93**, 66–71.
10. Zhou, A. G., Barsoum, M. W., Basu, S., Kalidindi, S. R. and El-Raghy, T., Incipient and regular kink bands in fully dense and 10 vol.% porous Ti_2AlC. *Acta Mater.*, 2006, **54**, 1631–1639.
11. Lin, Z. J., Zhou, Y. C., Li, M. S. and Wang, J. Y., In situ hot pressing/solid–liquid reaction synthesis of bulk Cr_2AlC. *Z. Metalkd.*, 2005, **96**, 291–296.
12. Tian, W. B., Wang, P. L., Zhang, G. J., Kan, Y. M., Li, Y. X. and Yan, D. S., Synthesis and thermal and electrical properties of bulk Cr_2AlC. *Scripta Mater.*, 2006, **54**, 841–846.
13. Gupta, S. and Barsoum, M. W., Synthesis and oxidation of V_2AlC and (Ti-0.5, V-0. 5)$_2$AlC in air. *J. Electrochem. Soc.*, 2004, **151**, D24–D29.
14. Salama, I., El-Raghy, T. and Barsoum, M. W., Synthesis and mechanical properties of Nb_2AlC and (Ti, Nb)$_2$AlC. *J. Alloys Compd.*, 2002, **347**, 271–278.
15. Salama, I., El-Raghy, T. and Barsoum, M. W., Oxidation of Nb_2AlC and (Ti, Nb)$_2$AlC in air. *J. Electrochem. Soc.*, 2003, **150**, C152–C158.
16. Sun, Z. M., Li, S., Ahuja, R. and Schneider, J. M., Calculated elastic properties of M_2AlC (M = Ti, V, Cr, Nb, and Ta). *Solid State Commun.*, 2004, **129**, 589–592.
17. Manoun, B., Gulve, R. P., Saxena, S. K., Gupta, S., Barsoum, M. W. and Zha, C. S., Compression behavior of M_2AlC (M = Ti, V, Cr, Nb, and Ta) phases to above 50 GPa. *Phys. Rev. B*, 2006, **73**(024110).
18. Lin, Z. J., Zhuo, M. J., Zhou, Y. C., Li, M. S. and Wang, J. Y., Microstructures and theoretical bulk modulus of layered ternary tantalum aluminum carbides. *J. Am. Ceram. Soc.*, 2006, **89**(12), 3765–3769.
19. Gupta, S., Filimonov, D. and Barsoum, M. W., Isothermal oxidation of Ta_2AlC in air. *J. Am. Ceram. Soc.*, 2006, **89**(9), 2974–2976.
20. Gupta, S., Filimonov, D., Palanisamy, T., El-Raghy, T. and Barsoum, M. W., Ta_2AlC and Cr_2AlC Ag-based composites—new solid lubricant materials for use over a wide temperature range against Ni-based superalloys and alumina. *Wear*, 2007, **262**, 1479–1489.
21. Bao, Y. W. and Zhou, Y. C., A new method for precracking beam for fracture toughness experiments. *J. Am. Ceram. Soc.*, 2006, **89**(3), 1118–1121.
22. Bao, Y. W., Chen, J. X., Wang, X. H. and Zhou, Y. C., Shear strength and shear failure of layered machinable Ti_3AlC_2 ceramics. *J. Eur. Ceram. Soc.*, 2004, **24**, 855–860.
23. Barsoum, M. W., Zhen, T., Kalidindi, S., Radovic, M. and Murugaiah, A., Fully reversible dislocation-based deformation of Ti_3SiC_2 to 1 GPa. *Nature Mater.*, 2003, **2**, 107–111.
24. Barsoum, M. W., Farber, L. and El-Raghy, T., Dislocation, kink bands, and room-temperature plasticity of Ti_3SiC_2. *Met. Mater. Trans.*, 1999, **30A**, 1727–1738.
25. Procopio, A. T., Barsoum, M. W. and El-Raghy, T., Characterization of Ti_4AlN_3. *Met. Mater. Trans.*, 2000, **31A**, 333–337.
26. Barsoum, M. W., Yoo, H.-I., Polushina, I. K., Rud', V. Yu., Rud', Yu. V. and El-Raghy, T., Electrical conductivity, thermopower, and Hall effect of Ti_3AlC_2, Ti_4AlN_3, and Ti_3SiC_2. *Phys. Rev. B*, 2000, **62**, 10194–10198.
27. Clinton, D. J. and Morrell, R., Hardness testing of ceramic materials. *Mater. Chem. Phys.*, 1987, **17**, 461–473.
28. Hirao, K. and Tomozawa, M., Microhardness of SiO_2 glass in various environments. *J. Am. Ceram. Soc.*, 1987, **70**, 497–502.
29. Quinn, J. B. and Quinn, G. D., Indentation brittle of ceramics: a fresh approach. *J. Mater. Sci.*, 1997, **32**, 4331–4346.
30. Low, I. M., Vickers contact damage of micro-layered Ti_3SiC_2. *J. Eur. Ceram. Soc.*, 1998, **18**, 709–713.
31. Bao, Y. W., Hu, C. F. and Zhou, Y. C., Damage tolerance of nanolayer-grained ceramic: a quantitative estimation. *Mater. Sci. Technol.*, 2006, **22**, 227–230.
32. Goldsby, J. C., Temperature-dependent elastic and anelastic behavior of silicon-based fiber-reinforced silicon carbide ceramic matrix composites. *Mater. Sci. Eng. A*, 2000, **279**, 266–274.
33. Bao, Y. W., Wang, X. H., Zhang, H. B. and Zhou, Y. C., Unusual thermal shock behaviors of Ti_3AlC_2 quenching in air and water from 200 to 1300 °C. *J. Eur. Ceram. Soc.*, 2005, **25**, 3367–3374.